1. Experimental details

1.1. General Methods

All reagents and solvents were obtained from commercial sources and used without further purification. Dry solvents were purchased from Acros Organics. 6,7-Dimethoxy-1,3-dithiolo[4,5-*b*][1,4]benzodithiin-2-thione (**3**) was synthesised according to a literature procedure.[1] Thin-layer chromatography was performed on silica gel-coated plates with fluorescent indicator F254 (Merck). For column chromatography, silica gel (0.04-0.063 mm, Merck) was used. ^{1}H and ^{13}C NMR experiments were performed on a JEOL ECX 400 or a Bruker AVANCE 700 instrument. Solvent residue signals were used as the internal standard. All shifts are reported in ppm and NMR multiplicities are abbreviated as s (singlet), d (doublet), t (triplet), m (multiplet) and br (broad). Coupling constants *J* are reported in Hertz. High-resolution ESI mass spectra were measured on an Agilent 6210 ESI-TOF device (Agilent Technologies). Melting points were determined on a SMP 30 (Stuart) instrument and are uncorrected.

1.2. Synthesis

6,7-Dimethoxy-1,3-dithiolo[4,5-*b*][1,4]benzodithiin-2-thione (3)

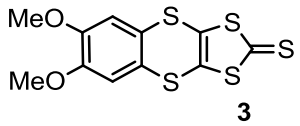

3

Under argon atmosphere, 1,2-diiodo-4,5-dimethoxybenzene (470 mg, 1.20 mmol), bis(tetrabutylammonium) bis(1,3-dithiole-2-thione-4,5-dithiolato)zinc (540 mg, 0.57 mol), Cu_2O (16 mg, 0.11 mmol), ethyl acetoacetate (30 µL, 0.23 mmol) and *N*,*N*-dimethylformamide (5.7 mL) were placed into a flame-dried Schlenk tube and the mixture was stirred at 80 °C overnight. Afterwards, the mixture was diluted with CH_2Cl_2 (50 mL) and washed with water (3x50 mL) and brine (50 mL). The organic phase was dried over $MgSO_4$ and the residue was purified using column chromatography (SiO_2, pentane/CH_2Cl_2 1:1, $R_f \approx$ 0.30). The crude product was recrystallised from acetonitrile and $CHCl_3$ to give thione **3** as yellow crystals (260 mg, 0.78 mmol, 65%). ^{1}H NMR (400 MHz, $CDCl_3$, 298 K): δ = 6.95 (s, 2H, H_{Ar}), 3.89 (s, 6H, OMe) ppm. ^{1}H NMR data are consistent with literature.[1]

2-(4,5-Bis(methylthio)-1,3-dithiol-2-ylidene)-6,7-dimethoxybenzo[*b*][1,3]dithiolo[4,5-*e*][1,4]dithiine (VTTF)

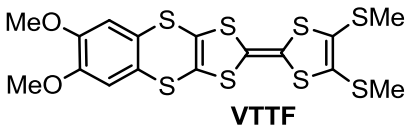

VTTF

6,7-Dimethoxy-1,3-dithiolo[4,5-*b*][1,4]benzodithiin-2-thione (**3**) (777 mg, 2.34 mmol) and 4,5-bis(methylthio)-1,3-dithiol-2-one (491 mg, 2.34 mmol) were dispersed in dry triethylphosphite (40 mL) under argon atmosphere. The mixture was heated to 90 C overnight. After cooling to room temperature, CH_3OH (80 mL) was added and the flask was placed in a freezer for 3 days. The precipitate was filtered off and purified by column chromatography (SiO_2, pentane/CH_2Cl_2 = 1:1). The product was recrystallised twice, from CH_3CN and $CHCl_3$, to give the desired product as yellow crystals (419 mg, 0.85 mmol, 36%). R_f = 0.25 in pentane/CH_2Cl_2 = 1:1; m. p. 197 °C; ^{1}H NMR (700 MHz, CD_2Cl_2, 298 K): δ = 6.92 (s, 2H, H_{Ar}), 3.82 (s, 6H, OMe), 2.42 (s, 6H, SMe) ppm; ^{13}C NMR (176 MHz, CD_2Cl_2): δ = 150.0, 128.0, 126.5, 124.1, 116.7, 113.4, 112.4, 56.7, 19.6 ppm; ESI-HRMS: *m/z* calcd. for $C_{16}H_{14}O_2S_8$: 516.8652 $[M+Na]^+$, found: 516.8666.

2. EPR measurements

CW EPR spectra at X-band frequency (ca. 9.5 GHz) were obtained with a Magnettech MS-5000 benchtop EPR spectrometer equipped with a rectangular TE 102 cavity and TC HO4 temperature controller. The measurements were carried out in synthetic quartz glass tubes. Dry and freshly distilled CH_3CN was used. Sample preparation and measurements were performed under nitrogen atmosphere. For the preparation of the radical-cation **VTTF** $^{\bullet+}$, 1.0 equiv. of $Fe(ClO_4)_3$ was added to a CH_3CN solution of **VTTF** (0.20 mM). The solution turned immediately dark brown because of the absorption of the radical-cation **VTTF**$^{\bullet+}$. We followed the procedure of EPR radical-cation dimerisation experiments reported eleswhere.[2] Briefly, the EPR signal intensity, measured at different temperatures by integration, was used to calculate the monomer fraction α_M. The α_M value decreases with lower temperatures due to the formation of the EPR-silent radical-cation dimer (**VTTF**$^{\bullet+}$)$_2$. For the correction of Curie law effects, 2,2,6,6-tetramethylpiperidinyloxyl (TEMPO) was used as reference. The experimental α_M values were fitted with Origin Pro 8 (OriginLab) according to equation 1:

$$\alpha_{\mathrm{M}} = -1 + \frac{\sqrt{1+8e^{\left(\frac{-H+T\cdot S}{RT}\right)}[\mathbf{VTTF}^{\bullet+}]}}{4e^{\left(\frac{-H+T\cdot S}{RT}\right)}[\mathbf{VTTF}^{\bullet+}]} \qquad \text{eq. (1)}$$

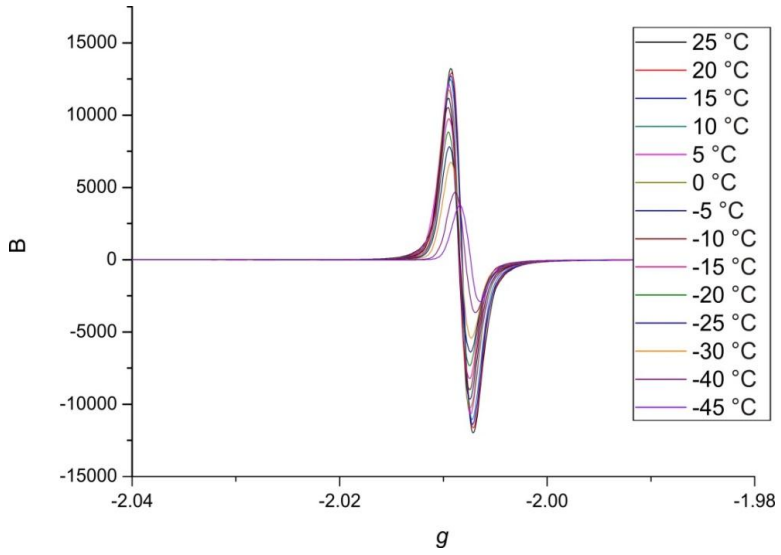

Fig. S1 EPR signal of **VTTF**$^{\bullet+}$ (0.20 mM, CH_3CN) at different temperatures. No precipitation was observed irrespective of the temperature.

3. UV/Vis-NIR measurements and spectroelectrochemistry

UV/Vis spectra of **VTTF** were recorded on a Cary 50 Bio photospectrometer (Varian) equipped with a xenon lamp. UV/Vis-NIR measurements were performed on an Avantes spectrometer with an AvaLight-DH-S-Bal light source, an AvaSpec-ULS2048 UV/Vis detector, and an AvaSpec-NIR256-TEC NIR detector. CH_3CN and CH_2Cl_2 with HPLC grade and Suprasil glass cuvettes with a path-length of 1, 0.5 or 0.1 cm were used. Spectroelectrochemical measurements were carried out in an optically transparent thin-layer electrochemical (OTTLE) cell (CaF_2 windows) with a platinum-mesh working electrode, a platinum-mesh counter electrode, and a silver-foil pseudoreference electrode. Voltammetric cycles between 0 and 1 V (vs silver pseudoreference) were performed.

Due to the low solubility of neutral **VTTF** in CH_3CN, a photometric titration to investigate the mixed-valence dimer was done in CH_2Cl_2. Addition of neutral **VTTF** to previously generated **VTTF**$^{\bullet+}$ leads to an emergent weak band (> 1300 nm) with no clear maximum as shown in Fig. S4. The rather unstructured and weak NIR band may at first sight come as a surprise. However, this characteristic band was also observed in spectroelectrochemistry measurements and in a CH_2Cl_2/CH_3CN mixture (1:1) as shown in Fig. S5. Furthermore, mixed-valence complexes of tetrathiafulvalene which exhibit very similar charge resonance bands were previously reported.[3-5] The binding constant of the

mixed-valence complex $(\mathbf{VTTF_2})^{\bullet+}$ K_{MV} in CH_2Cl_2 was obtained by non-linear curve fitting of a 1:1 binding model as described earlier[6] with the program Origin Pro (OriginLab) according to equation 2 taking the dilution of $[\mathbf{VTTF}^{\bullet+}]_0$ into account. The binding constant K_{MV} was averaged from the fit of four different wavelengths (1600, 1800, 2000, and 2200 nm).

$$\Delta A_{obs} = \epsilon \frac{1}{2}\left([\mathbf{VTTF}]_0 + [\mathbf{VTTF}^{\bullet+}]_0 + \frac{1}{K_{MV}} - \sqrt{\left([\mathbf{VTTF}]_0 + [\mathbf{VTTF}^{\bullet+}]_0 + \frac{1}{K_{MV}}\right)^2 + 4[\mathbf{VTTF}]_0[\mathbf{VTTF}^{\bullet+}]_0}\right) \quad \text{eq. (2)}$$

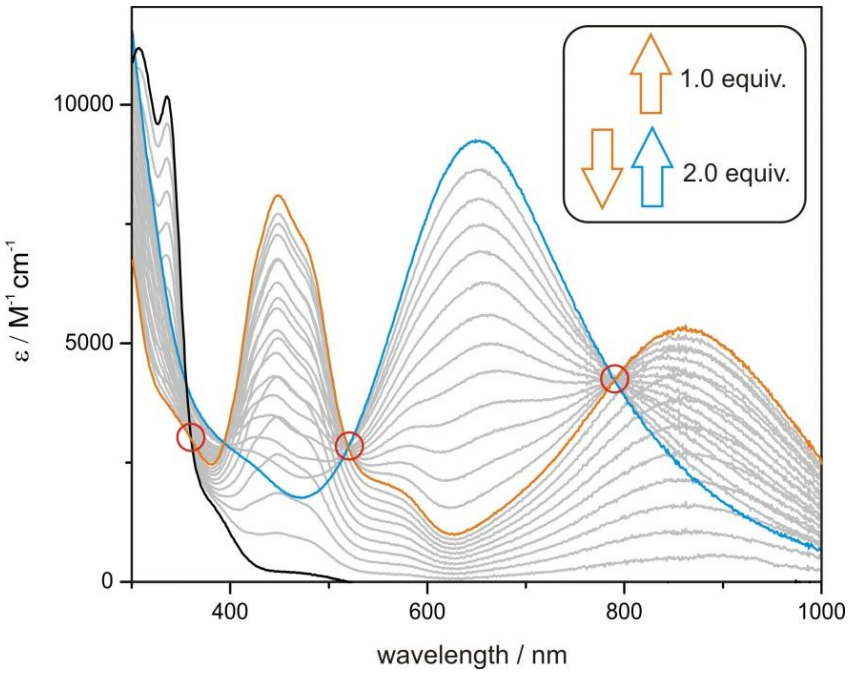

Fig. S2 Photometric UV/Vis titration of **VTTF** (5 10^{-5} M, CH_3CN, 298 K) with one-electron oxidant $Fe(ClO_4)_3$. The black curve corresponds to neutral **VTTF** (0.0 equiv. oxidant), the orange curve to its radical-cation **VTTF** $^{\bullet+}$ (1.0 equiv. oxidant) and the blue curve to the fully oxidised dication **VTTF** $^{2+}$ (2.0 equiv. oxidant). The clear-cut isosbestic points (red circles) confirm a clean transition between all three oxidation states.

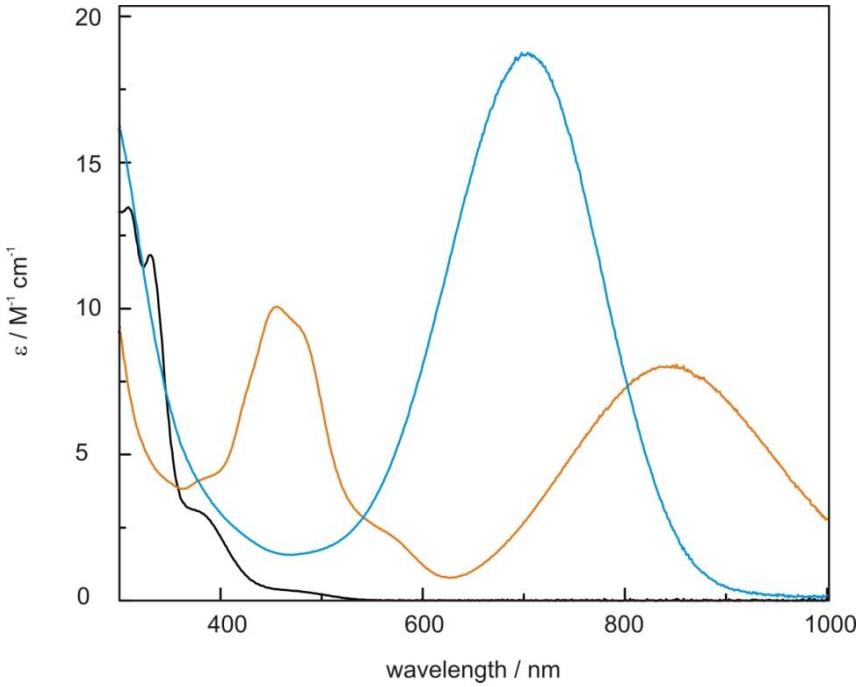

Fig. S3 UV/Vis spectra (5 10^{-5} M, CH_3CN, 298 K) of **TMT-TTF** in oxidation state 0 (black), +1 (orange), and +2 (blue). The oxidised species were generated by addition of $Fe(ClO_4)_3$.

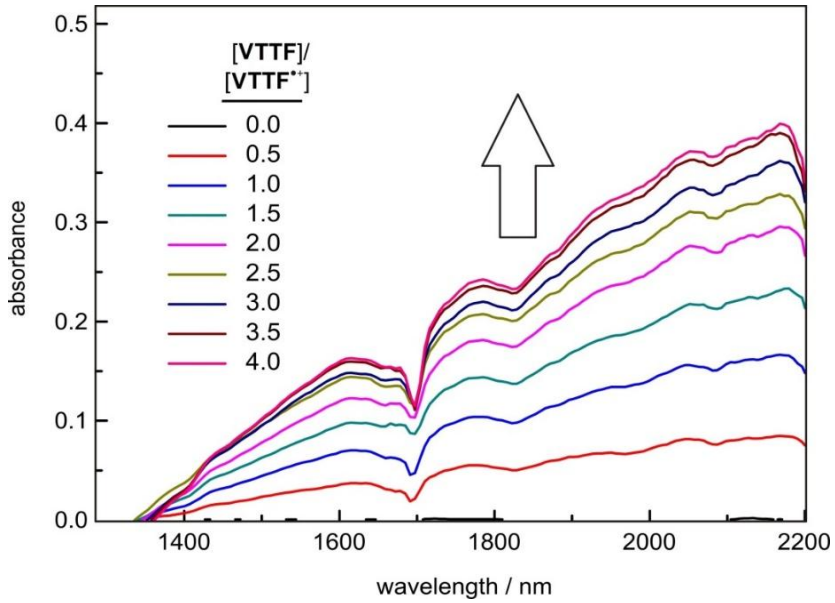

Fig. S4 Photometric NIR titration of **VTTF**$^{\bullet+}$ (5.0 mM, CH_2Cl_2, 298 K) with a concentrated CH_2Cl_2 solution (50 mM) of neutral **VTTF**. The emerging broad band > 1300 nm is caused by the formation of the mixed-valence (**VTTF**$_2$)$^{\bullet+}$ dimer.

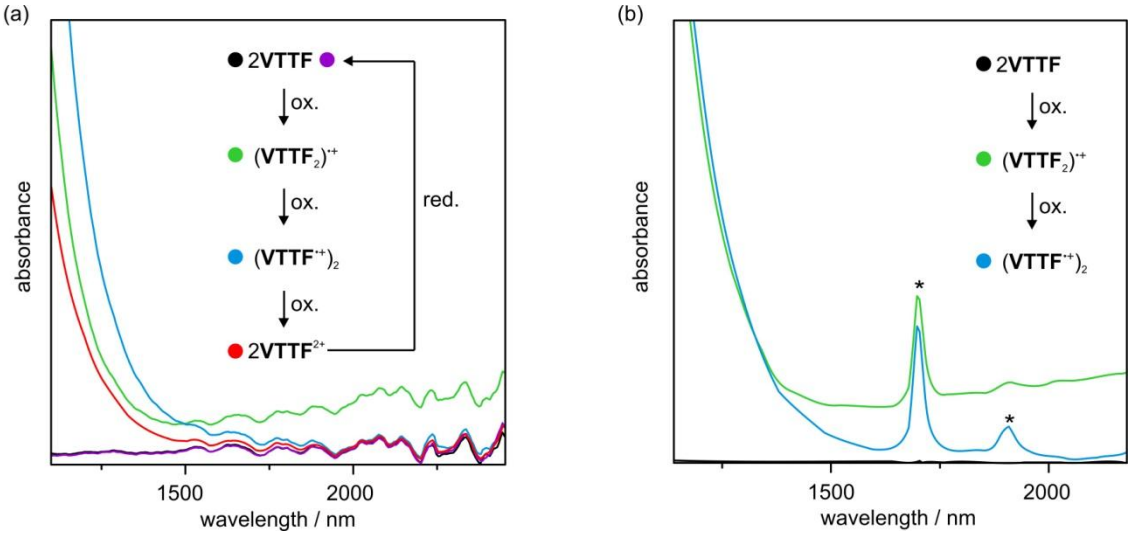

Fig. S5 (a) Changes of the NIR spectra of **VTTF** (30 mM, CH_2Cl_2, 298 K, 0.1 M *n*-Bu_4NPF_6) in the course of stepwise oxidation and reduction during spectroelectrochemistry. The results shows that only the mixed-valence state displays the broad NIR band > 1300 nm and that the oxidation/reduction process is fully reversible. (b) Changes of the NIR spectra during stepwise chemical oxidation of **VTTF** (30 mM, CH_2Cl_2/CH_3CN (1:1), 298 K) by addition of chemical oxidant $Fe(ClO_4)_3$. Artefacts are marked with an asterisk.

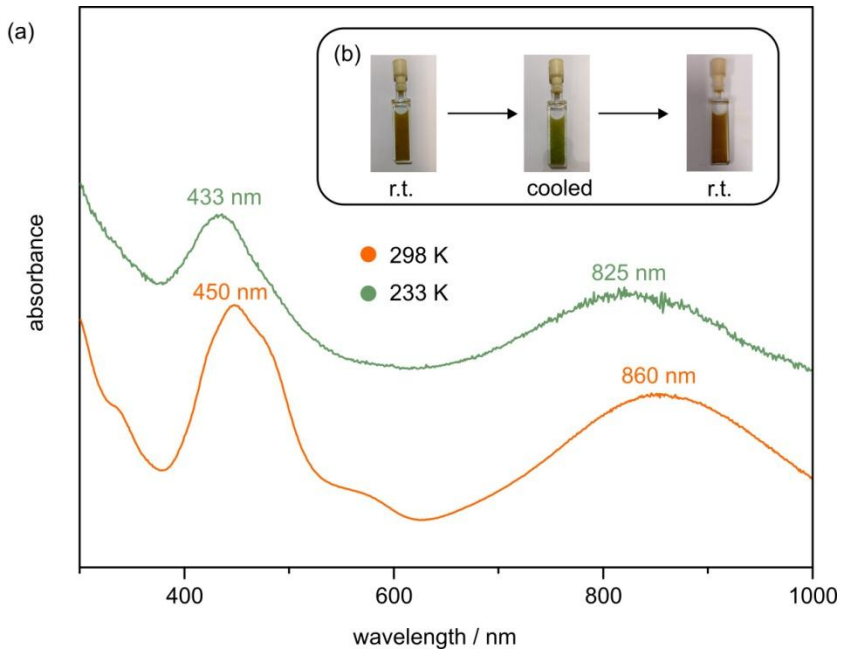

Fig. S6 (a) UV/Vis spectra (25 mM, CH_3CN,) of **VTTF**$^{\bullet+}$ at room temperature and 233 K. The oxidised monomeric **VTTF**$^{\bullet+}$ was chemically generated by addition of 1 equiv. $Fe(ClO_4)_3$. The broadening of bands for the 233 K measurement is due to slight precipitation in the cuvette. (b) Photographs of the cuvette before cooling, directly after cooling, and after warming up again to room temperature.

4. Electrochemical measurements

Cyclic Voltammetry (CV) and differential pulse Voltammetry (DPV) were performed on a PGSTAT302N potentiostat (Autolab) using a three-electrode configuration: a freshly polished glassy carbon working electrode, a platinum wire counter electrode and a silver wire pseudoreference electrode. All measurements were conducted twice, CV measurements in addition with a broad range of different scan rates (25 → 1000 mV s^{-1}) to ensure reversibility of the processes. The decamethylferrocene/decamethylferrocenium couple was used as the internal reference. Potentials were referenced against the ferrocene/ferrocenium (FcH/FcH^+) couple.[7] Dry and argon-purged solvents were used.

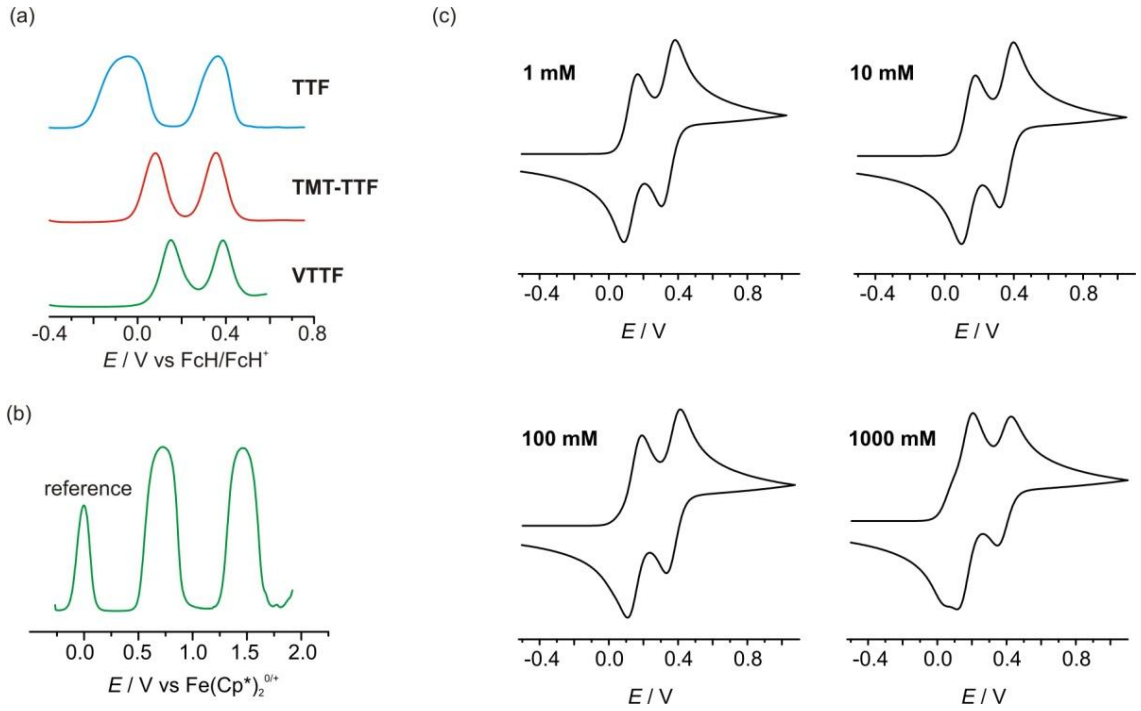

Fig. S7 (a) DPV measurements (10 mV s^{-1} scan rate, 25 mV modulation amplitude, 50 ms modulation time, 5 mV step potential, 0.5 s interval time) of **TTF, TMT-TTF** and **VTTF** (0.1 mM) in CH_3CN (0.1 M *n*-Bu_4NPF_6). (b) DPV measurements (10 mV s^{-1} scan rate, 25 mV modulation amplitude, 50 ms modulation time, 5 mV step potential, 0.5 s interval time) of **VTTF** (22 mM) in CH_2Cl_2 (0.1 M tetrabutylammonium tetrakis[3,5-bis(trifluoromethyl)phenyl]borate). (c) Simulated voltammograms (100 mV s^{-1}) for different initial concentrations of monomer **VTTF**. Note that a broadening/splitting of the first redox wave emerges in the molar concentration range.

Regarding the voltammetric behavior of **VTTF**, mixed-valence complexes, for example covalently[8] or strongly non-covalently bound (e.g. K_{MV} = 10^4 M^{-1})[9] organic redox-active molecules, usually show a splitting or at least a broadening of the first redox-wave. However, even in more concentrated CH_2Cl_2 solution (Fig. S7b) using tetrabutylammonium

tetrakis[3,5-bis(trifluoromethyl)phenyl]borate as weakly-coordinating[10] electrolyte, we could not observe a distinct splitting of the first transition. To unravel, why this is not observed for **VTTF** and its corresponding mixed-valence complex (**VTTF**$_2$)$^{\bullet+}$, we conducted digital simulations (DigiElch Professional software package)[11] based on the determined redox-potentials and equilibrium constants which are depicted in Figure S7c. We estimate that a broadening effect of the first wave could emerge in the molar range. Common measuring concentrations and a window for reliable data for our CV and DPV set up is approximately 0.1-20 mM analyte concentration. The absence of visible features in the voltammograms does not exclude partial presence of the mixed-valence dimer in solution.

5. Computational details

Structure optimisations of **VTTF** and its dimers in their 0, 1+, and 2+ charge state at the TPSS-D3(BJ)/def2-TZVP[12-15] level of DFT employing the RI-*J* approximation[16] for the Coulomb term and COSMO[17] (ε = 36.6) for simulating implicit solvent effects were performed using the Turbomole 7.0.1[18] programme package. Minima were ascertained by frequency analyses showing no imaginary frequencies. Most of the subsequent single point calculations were done at the PBE0-D3(BJ)/def2-TZVP[19] level employing the RI*J*COSX[20] approximation and incorporating implicit solvent effects with CPCM (ε = 36.6)[21] using ORCA 4.0.0.[22] These included the computation of the spin densities of (**VTTF**$_2$)$^{\bullet+}$ and **VTTF**$^{\bullet+}$ (Fig. S7) and the prediction of UV/Vis absorption spectra in the framework of linear-response time-dependent DFT (Fig. 4). Furthermore, free enthalpies of association ΔG_a were calculated according to

$$\Delta G_{\mathrm{a}} = \Delta E + \Delta G_{\mathrm{RRHO}} + \Delta G_{\mathrm{solv}}$$

where ΔE is the electronic binding energy of the dimer calculated *in vacuo* at the PBE0-D3(BJ)/def2-QZVP[23] level. Note that the BSSE is not accounted for, since the quadruple-zeta basis set is assumed to be near the basis set limit for these kinds of DFT calculations.[24] ΔG_{RRHO} was obtained from calculated frequencies using standard statistical thermodynamic approaches, whereas low-lying vibrational modes were corrected via the so-called *rigid-rotor harmonic-oscillator ansatz* proposed by Grimme.[25] The last term, ΔG_{solv}, represents the contribution from the dissolution of the dimer in comparison to two dissolved monomers. ΔG_{solv} was computed with the COSMOThermX programme suite[26,27] applying the COSMO-RS scheme[28,29] with BP86/def-TZVP[30-32] parametrisation. Table S1 summarises the various contributions to ΔG_a for both (**VTTF**$_2$) $^{\bullet+}$ and (**VTTF**$^{\bullet+}$)$_2$. Discrepancies between the two dimers are explained by electrostatic repulsions in the gas-phase present in (**VTTF**$^{\bullet+}$)$_2$ and a significant charge stabilisation in solution.

(a) (b)

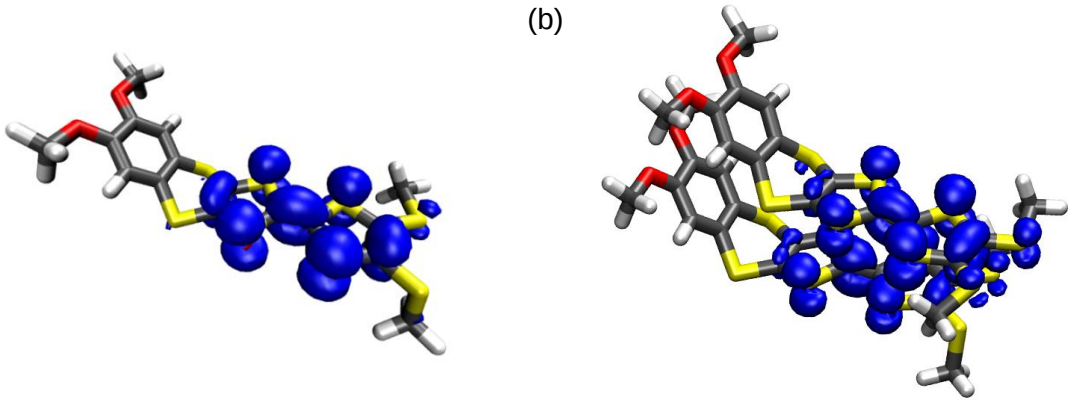

Fig. S8 Spin density of (a) **VTTF**$^{\bullet+}$ and (b) (**VTTF**$_2$)$^{\bullet+}$ dimer obtained at the PBE0-D3(BJ)/def2-TZVP level of DFT.

Table S1 Contributions to the free enthalpies of association, ΔG_a, data given in kJ mol^{-1}.

	ΔE	ΔG_{RRHO}	ΔG_{solv}	ΔG_a
(**VTTF**$_2$)$^{\bullet+}$	-144.7	86.3	54.2	- 4.3
(**VTTF**$^{\bullet+}$)$_2$	62.4	88.1	-136.8	13.6

6. Crystallographic data and electrocrystallisation

The electrocrystallisation of [**VTTF**](BF$_4$)$_2$ was conducted using a custom made H-cell which consists of two glass compartments separated by a glass frit. A solution of 12 mg (24 µmol, 12 µmol per compartment) **VTTF** and 100 mg (0.3 mmol) *n*-Bu$_4$NBF$_4$ in CH$_2$Cl$_2$ (20 mL) was distributed equally to both compartments. After closing the apparatus with two septa, a platinum wire was submerged into the solution in each compartment. The wires then acted as the electrodes for a self-made constant current source. A current of 1 µA was applied over 10 days, until a black solid appeared on the anode, from which a dark green crystal of a [**VTTF**](BF$_4$)$_2$ salt suitable for X-ray diffraction could be harvested. The applied current and the duration of electrolyses (0.86 C = 8.96 µmol) are not sufficient to quantitatively oxidise **VTTF** in solution to the corresponding dication **VTTF**^{2}. However by turning brown, the solution indicated the formation of a partly soluble radical-cationic species. Due to the non-polar nature of CH$_2$Cl$_2$ and most certainly a lower solubility of the fully oxidised **VTTF**$^{2+}$, we assume that the dication precipitates at the anode and, thus, is removed from the electrochemical disproportionation equilibrium according to an *EEC*$_i$ mechanism.

The data for [**VTTF**](BF$_4$)$_2$ were collected on an Agilent SuperNova single-source diffractometer equipped with an Eos CCD detector at 120(2) K using mirror-monochromated Mo-*K*α (λ = 0.71073 Å) radiation. Data collection and reduction was performed using the program *CrysAlisPro*.[33] The analytical face-indexing-based absorption correction method was

applied. The structure was solved by intrinsic phasing methods (*SHELXT*[34]) and refined by full-matrix least squares on F^2 using *WinGX*[35] which utilises the *SHELXL*-2017/1[36] module. All hydrogen atoms were constrained to their idealised positions and refined using riding models with U_{eq}(H) of 1.5U_{eq}(C) for terminal methyl groups, and of 1.2 of U_{eq}(C) for other groups.

Crystal data of [**VTTF**](BF$_4$)$_2$: $C_{16}H_{14}B_2F_8O_2S_8$, M = 668.37, monoclinic, space group $P2_1/n$ (no.14), a = 10.7366(4), b = 11.0614(5), c = 21.0424(11) Å, β = 101.460(4)°, V = 2449.2(2) Å^3, Z = 4, ρ_{calc} = 1.813 Mgm^{-3}, μ = 0.807 mm^{-1}, F(000) = 1344, θ range = 2.98-29.81°, 10396 reflections collected, 6081 unique (R_{int} = 0.0275, I>2σ(I) = 4696), which were used in all calculations (329 parameters), Goodness-of-fit (F^2) = 1.025. The final R indices [I>2σ(I)]: R1 = 0.0386 and wR2 = 0.0800. R indices (all data): R1 = 0.0578 and wR2 = 0.0892. Largest residual electron densities: 0.435 and -0.359 e.Å^{-3}.

X-ray data of neutral **VTTF** were collected on a Bruker D8 Venture system at 100(2) K using graphite-monochromated $Cu_{K\alpha}$ radiation (λ_α = 1.54178 Å). The strategy for the data collection was evaluated by using the *APEX2* software.[37] The data were collected by the standard omega + phi scan techniques, and were scaled and reduced using *Saint+* and *SADABS* software.[38,39] The structures were solved by intrinsic phasing methods using *SHELXT*-2014/7.[34] Structures were refined by full matrix least-squares using *SHELXL*-2014/7, refining on F^2.[36,40] Non-hydrogen atoms were refined anisotropically.

Crystal data of **VTTF**: $C_{16}H_{14}O_2S_8$ (M = 494.75 g/mol): monoclinic, space group $P2_1/c$ (no. 14), a = 31.7792(12) Å, b = 4.5304(2) Å, c = 14.5020(6) Å, β = 101.1090(10)°, V = 2048.77(15) Å^3, Z = 4, T = 100(2) K, μ(CuKα) = 8.164 mm-1, ρ_{calc} = 1.604 g/cm3, 17424 reflections measured (8.506° ≤ 2Θ ≤ 144.864°), 4028 unique (R_{int} = 0.0368, R_{sigma} = 0.0319) which were used in all calculations. The final R1 was 0.0302 (I > 2σ(I)) and wR2 was 0.0836 (all data). Largest residual electron densities: 0.49 and -0.33 e.Å^{-3}.

7. ^{1}H, ^{13}C NMR and HR mass spectra

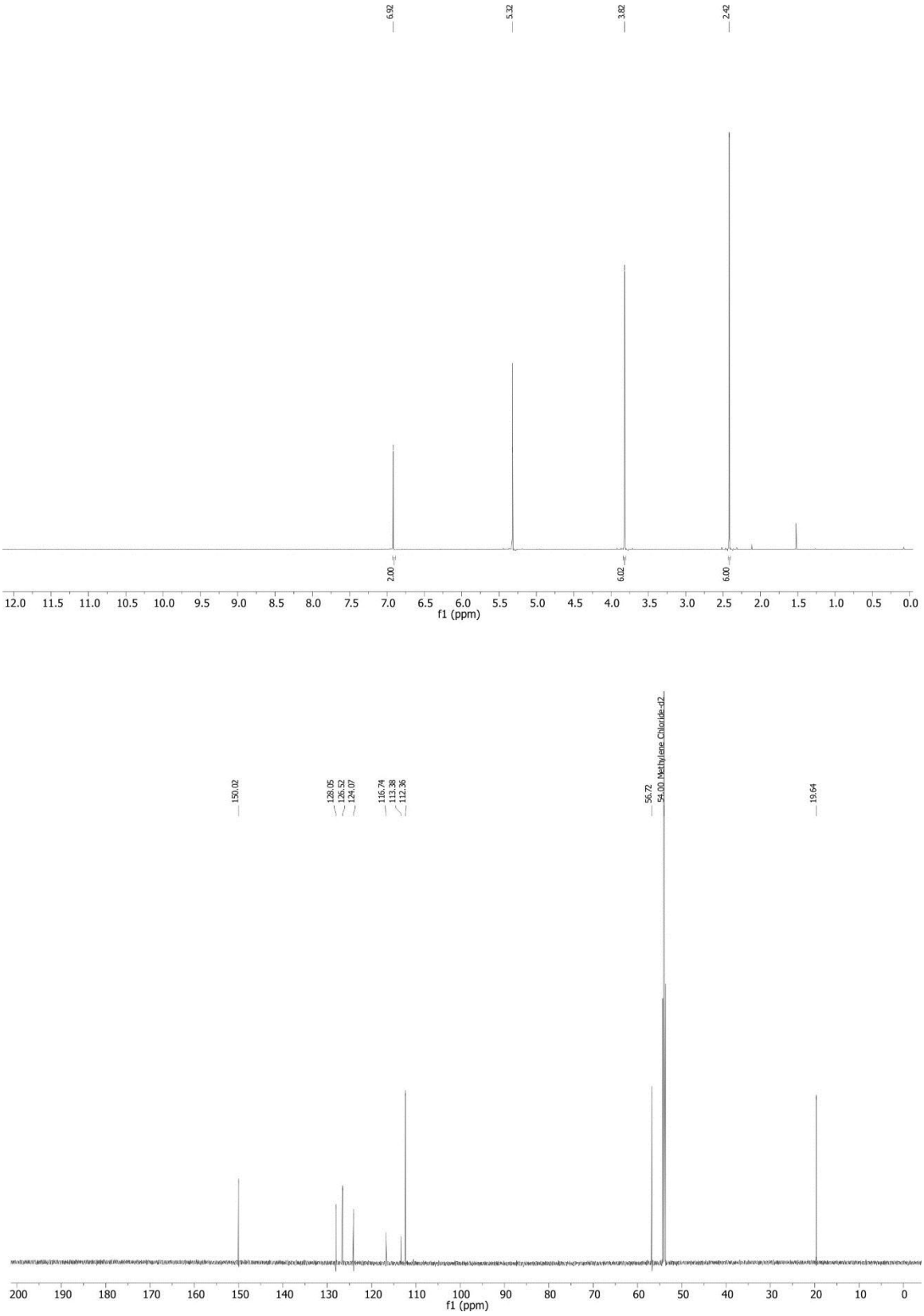

Fig. S9 ^{1}H (top) and ^{13}C (bottom) NMR spectrum (700/176 MHz, CD_2Cl_2, 298 K) of **VTTF**.

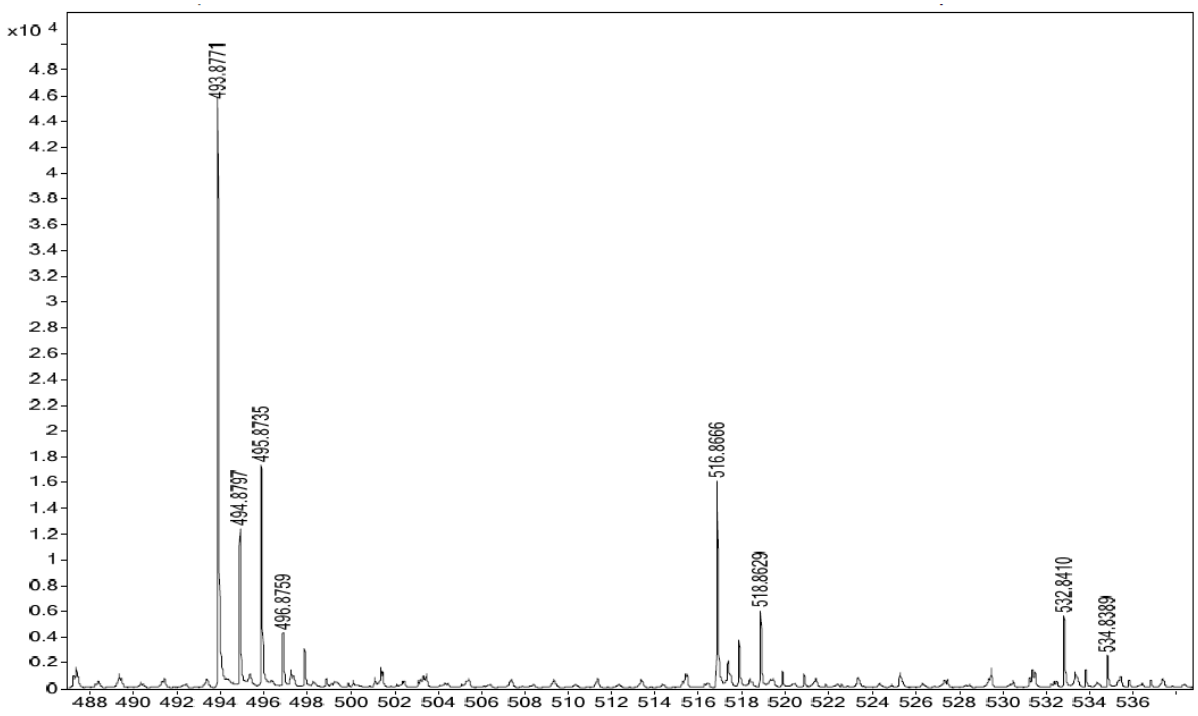

Fig. S10 ESI high-resolution mass spectrum of **VTTF** (positive mode, MeOH).

8. References

1 J. Sun, X. Lu, J. Shao, Z. Cui, Y. Shao, G. Jiang, W. Yu and X. Shao, *RSC Adv.*, 2013, **3**, 10193.

2 J. M. Lu, S. V. Rosokha and J. K. Kochi, *J. Am. Chem. Soc.*, 2003, **125**, 12161.

3 G. Barin, A. Coskun, D. C. Friedman, M. a Olson, M. T. Colvin, R. Carmielli, S. K. Dey, O. A. Bozdemir, M. R. Wasielewski and J. F. Stoddart, *Chem. Eur. J.*, 2011, **17**, 213.

4 A. Coskun, J. M. Spruell, G. Barin, A. C. Fahrenbach, R. S. Forgan, M. T. Colvin, R. Carmieli, D. Benitez, E. Tkatchouk, D. C. Friedman, A. A. Sarjeant, M. R. Wasielewski, W. A. Goddard III and J. F. Stoddart, *J. Am. Chem. Soc.*, 2011, **133**, 4538-4547.

5 M. Hasegawa, J.-I. Takano, H. Enozawa, Y. Kuwatani and M. Iyoda, *Tetrahedron Lett.,* 2004, **45**, 4109.

6 P. Thordarson, *Chem. Soc. Rev.*, 2011, **40**, 1305.

7 J. R. Aranzaes, M.-C. Daniel and D. Astruc, *Can. J. Chem.*, 2006, **84**, 288.

8 M. Hasegawa, K.-I. Nakamura, S. Tokunaga, Y. Baba, R. Shiba, T. Shirahata, Y. Mazaki and Y. Misaki, *Chem. Eur. J.*, 2016, **22**, 10090.

9 M. A. Christensen, C. R. Parker, T. J. Sørensen, S. de Graaf, T. J. Morsing, T. Brock-Nannestad, J. Bendix, M. M. Haley, P. Rapta, A. Danilov, S. Kubatkin, O. Hammerich and M. B. Nielsen, *J. Mater. Chem. C*, 2014, **2**, 10428.

10 W. E. Geiger and F. Barrière, *Acc. Chem. Res.*, 2010, **43**, 1030.

11 DigiElch Professional Version 7.FD 2006, ElchSoft GbR, Kleinromstedt, Germany.
12 J. Tao, J. P. Perdew, V. N. Staroverov and G. E. Scuseria, *Phys. Rev. Lett.*, 2003, **91**, 146401.
13 S. Grimme, J. Antony, S. Ehrlich and H. Krieg, *J. Chem. Phys.*, 2010, **132**, 154104.
14 S. Grimme, S. Ehrlich and L. Goerigk, *J. Comput. Chem.*, 2011, **32**, 1456.
15 K. Eichkorn, F. Weigend, O. Treutler and R. Ahlrichs, *Theor. Chem. Acc.*, 1997, **97**, 119.
16 K. Eichkorn, O. Treutler, H. Öhm, M. Häser and R. Ahlrichs, *Chem. Phys. Lett.*, 1995, **240**, 283.
17 A. Klamt and G. Schüürmann, *J. Chem. Soc., Perkin Trans. 2*, 1993, 799.
18 R. Ahlrichs, M. Bär, M. Häser, H. Horn and C. Kölmel, *Chem. Phys. Lett.*, 1989, **162**, 165.
19 J. P. Perdew, M. Ernzerhof and K. Burke, *J. Chem. Phys.*, 1996, **105**, 9982.
20 F. Neese, F. Wennmohs, A. Hansen and U. Becker, *Chem. Phys.*, 2009, **356**, 98.
21 V. Barone and M. Cossi, *J. Phys. Chem. A* 1998, **102**, 1995.
22 F. Neese, *Wiley Interdiscip. Rev. Comp. Mol. Sci.*, 2012, **2**, 73.
23 F. Weigand and R. Ahlrichs, *Phys. Chem. Chem. Phys.* 2005, **7**, 3297.
24 C. J. Cramer, *Essentials of computational chemistry: theories and models*, Wiley, Chichester, West Sussex, England; Hoboken, NJ, 2nd edition, **2004**.
25 S. Grimme, *Chem. Eur. J.*, 2012, **18**, 9955.
26 COSMOtherm, C3.0, release 1602, COSMOlogic GmbH & Co KG, http://www.cosmologic.de
27 F. Eckert and A. Klamt, *AlChE J*, 2002, **48**, 369.
28 A. Klamt, *J. Phys. Chem.*, 1995, **99**, 2224.
29 A. Klamt, V. Jonas, T. Bürger and J. C. Lohrenz, *J. Phys. Chem. A*, 1998, **102**, 5074.
30 A. D. Becke, *Phys. Rev. A*, 1988, **38**, 3098.
31 J. P. Perdew, *Phys. Rev. B*, 1986, **33**, 8822.
32 A. Schäfer, C. Huber and R. Ahlrichs, *J. Chem. Phys.*, 1994, **100**, 5829.
33 *CrysAlisPro* (Version 1.171.38.41.), Rigaku Oxford Diffraction, 2015.
34 G. M. Sheldrick, *Acta Crystallogr., Sect. A: Found. Adv.*, 2015, **71**, 3.
35 L. J. Farrugia, *J. Appl. Crystallogr.*, 2012, **45**, 849.
36 G. M. Sheldrick, *Acta Crystallogr., Sect. C: Struct. Chem.*, 2015, **71**, 3.
37 Bruker, APEX2, Bruker AXS Inc., Madison, WI, 2012.
38 SAINT+ (Data Integration Engine, Version 8.27b), Bruker AXS Inc., Madison, WI, 1997-2012.
39 G. M. Sheldrick, SADABS (Ver. 2008/1), Bruker AXS Inc., Göttingen, Germany, 2008.

40 (a) G. M. Sheldrick, *Acta Cryst. Sect A.*, 2008, **64**, 112; (b) C. B. Hübschle, G. M. Sheldrick and B. Dittrich, *J. Appl. Cryst.* 2011, **44**, 1281; (c) G. M. Sheldrick, SHELXL (Version 2014/7), Bruker AXS Inc., Göttingen, Germany, 2014.